Vacuum 150 (2018) 144–154

Contents lists available at ScienceDirect

Vacuum

journal homepage: www.elsevier.com/locate/vacuum

Tailoring of titanium thin film properties in high power pulsed magnetron sputtering

Baohua Wu [a, b], Yan Yu [a], Jian Wu [a], Ivan Shchelkanov [b], David N. Ruzic [b], Nan Huang [a], Y.X. Leng [a, *]

[a] Key Laboratory of Advanced Technologies of Materials, Ministry of Education of China, School of Materials Science and Engineering, Southwest Jiaotong University, Chengdu 610031, China
[b] Center for Plasma-Material Interactions, Department of Nuclear, Plasma, and Radiological Engineering, University of Illinois at Urbana-Champaign, Urbana, IL 61801, USA

ARTICLE INFO

Article history:
Received 31 October 2017
Received in revised form
20 January 2018
Accepted 22 January 2018
Available online 6 February 2018

Keywords:
Tailoring of film properties
High Power Pulsed Magnetron Sputtering (HPPMS)
Average target power
Peak target power
Ion-to-atom ratio

ABSTRACT

Ti films are widely used in electrical engineering, biomedical instrumentation, and other industries owing to their excellent material properties. High Power Pulsed Magnetron Sputtering (HPPMS) is a promising physical vapor deposition (PVD) technique used for producing highly ionized target species, thereby opening the possibility of controlling the material properties of the growing films. Controlling the thin film properties helps achieve high quality films to cater the needs of a specific application. In this study, Ti films properties were tailored by controlling the peak and average target power values in HPPMS. The effect of peak and average target power on the plasma composition above the substrate was systematically studied. For a constant average power, the increase in the peak power significantly raises the ion-to-atom ratio and density of the plasma flux incident on the substrate. This leads to the Ti films exhibiting compressive stress, smaller grain size, and smoother surface at lower deposition rates. On the other hand, the increase in the average power at a constant peak power causes no remarkable change in the ion-to-atom ratio, but the overall magnitude of the number of metal ions and atoms and gas temperature around the substrate increase obviously. The Ti films deposited at high average powers were characterized by larger grain size with a highly preferred orientation of (002), rougher surface, and exhibited signs of tensile stress. The results obtained from this study provide guidelines for achieving high quality hard metal films with desired properties by manipulating the peak and average power in HPPMS discharge.

1. Introduction

Ti thin films are used in a wide variety of industries owing to their exceptional material properties such as superior strength, excellent thermal stability, and good corrosion resistance [1–5]. The material properties of Ti films determine the overall performance of the materials in the applications they are used. Ti films with a high surface roughness and large grain size exhibit a high optical reflectance [6], and Ti films with a low residual stress are essential for the preparation of stable TiO_2 nanotubes [7]. In order to improve the adhesion between thin films and the substrates, Ti films are used as an interlayer between the film and the substrate. For example, a thin layer of Ti is often used to improve the adhesion of Ti-O film on CoCrMo [8] and Cu film on Si [9]. Similarly, the adhesion of TiN on 15300 steel [10] and corrosion resistance of TiN on AISI D2 steel [11] can be improved by increasing the thickness of Ti interlayer. Moreover, Ti interlayer can is effective for changing the texture of the growing film. Strong (002) textured Ti films are necessary for changing the TiN film texture from (002) to (111) [12]. An improvement in the (002) texture of the Ti films has shown to enhance the (111) texture growth in the Al films [13]. In-depth understanding of the tailoring thin film properties such as thickness, texture, roughness, and residual stress is, thus, very important to meet the stringent requirements in various applications.

Recent studies have shown that high power pulsed magnetron sputtering (HPPMS) systems have great potential for tailoring the film properties [14,15]. HPPMS is a pulsed magnetron sputtering technique operating at high peak powers and low duty cycles to

* Corresponding author.
E-mail address: yxleng@263.net (Y.X. Leng).

https://doi.org/10.1016/j.vacuum.2018.01.039
0042-207X/

avoid target overheating. Owing to the high peak power, a dense plasma is created in front of the target surface, resulting in electron densities of up to 10^{19} m^{-3} and high degree of ionization of the sputtered material such as 90% in the case of Ti [16]. Having control over the flux and energy of the ionized target species incident the substrate increases the possibility to manipulate the crystal phases, microstructure, and chemical composition of the resultant films [17]. Thus, it is important to understand how to control the ion-to-atom ratio around the substrate to tailor the material properties of the growing Ti film.

It has been pointed out by A. Anders et al., that HPPMS is a kind of pulsed sputtering where the peak power exceeds the time-averaged power by typically two orders of magnitude [18]. The average target power ($\boldsymbol{P_{ave}}$) and peak target power ($\boldsymbol{P_{peak}}$) during the HPPMS discharge are two key deposition parameters altering the ion-to-atom ratio at the substrate. It was reported that the ion-to-atom ratio can be improved by the peak target power [19–24], but few of them focus on the effect of the average power. Meanwhile, HPPMS is often used to deposit smoother, denser and harder films [19–22], while preparing films with rough surface, large grain size or tensile stress is rarely studied, which is also important for the films applications. Therefore, in order to better tailor the properties of Ti film, films were deposited at various average and peak powers using HPPMS. The deposition rate, roughness, residual stress and microstructures were studied for each of case. A detailed comparative study of the effect of peak and average power on the ion-to-atom ratio at the substrate is presented, and the relationship between the ion-to-atom ratio and films properties is discussed.

2. Experimental details

Ti deposition experiments were performed in a laboratory-scale vacuum system with a base pressure lower than 1×10^{-3} Pa. Fig. 1 shows the schematic diagram of the deposition chamber used in this study. A detailed description of the experimental set-up was reported by B.H. Wu et al. [25]. In all our experiments, silicon (100) substrate and Chengdu Pulsetech Electrical (HPS-450D, China) HPPMS power supply was used for the Ti deposition. The HPPMS power supply was equipped with a resistor, R_1 of 3 Ω, which helped limit the plasma current and protect the power source from arcing. Four unbalanced magnetron plasma sources with rectangle planar titanium targets (134 × 175 mm^2) were placed inside a cylindrical-shaped vacuum chamber of 500 mm × 500 mm (diameter × height). The effective target area was approximately 42 cm^2, which was measured from the track of the discharge on the target surface. The substrate holder was located parallel to one of the titanium targets, and the distance between the target and substrate was 70 mm. The argon gas flow into vacuum chamber was controlled using a mass flow controller (MFC) to establish an operating pressure of 0.55 Pa. During deposition, there is no external heating or bias applied over the substrate. In order to compare the influence of the peak and average powers, experiments with varying pulse widths (shown in Table 1), frequencies (shown in Table 2), and voltages (shown in Table 3) were conducted. For the first two groups, the pulse width and frequency (shown in Tables 1 and 2) were changed to vary the average power, and the peak power was kept constant. In the third group of experiments (shown in Table 3), the discharge voltage and frequency were varied to control the peak power by keeping the average power constant. The experimental parameters used in this study are shown in Tables 1–3. During the depositions, the target voltage (V), discharge current (I) were measured using a digital oscilloscope (Tektronix, model TDS-220) with a voltage probe (Tektronix, model P-5100) and a current monitor (Pearson, Model 411), respectively. The average power ($\boldsymbol{P_{ave}}$) and peak power ($\boldsymbol{P_{peak}}$) were calculated from the measured discharge current and target voltage using the following equations.

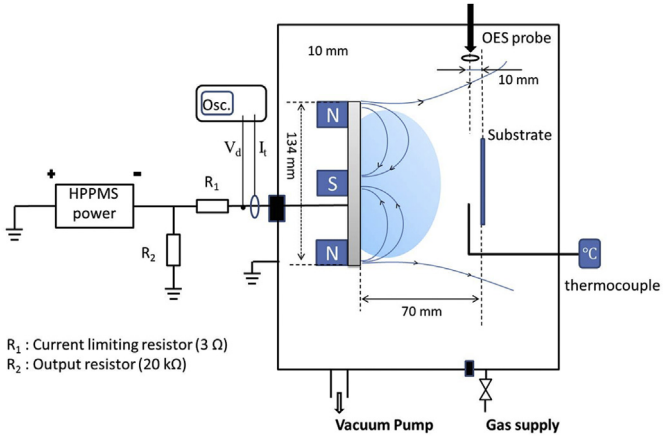

Fig. 1. Schematic of the deposition chamber.

$$P_{ave} = f \cdot \int U(t) \cdot I(t) dt, \quad (1)$$

$$P_{peak} = I_p \cdot U_s, \quad (2)$$

where f is the frequency (Hz), I_p is the peak current, and U_s is the stable target voltage as shown in Fig. 2. The calculated average and peak power values are shown in Tables 1–3. The ion current through the substrate was also measured with a current monitor (Pearson, Model 411). In order to get the ion saturation current, a negative 50 V bias was applied using a DC bias power supply to substrate in the plasma [26].

Optical emission spectroscopy (OES) was used to investigate the plasma composition at different conditions. Avantes, AvaSpec-2048-7-USB2 spectrometer was used for this purpose. The optical fiber connected to the spectrometer was placed outside the quartz window port, and it was positioned sideways to the chamber to monitor the discharge region, which is 10 mm from the substrate surface as shown in Fig. 1. An optical spectrum was recorded for wavelengths ranging from 200 nm to 820 nm, and the measured spectra were analyzed using a spectrum analyzer (Avantes, AvaLIBS Specline-AMS). The gas temperature around the substrate was recorded using a thermocouple, and the top of the thermocouple was placed at about 10 mm from the substrate surface.

In order to compare the effect of peak power and average power on films properties further, the Ti films were deposited at different peak power and average power. The peak power and average power were varied by trigger voltages and pulse widths, separately. The deposited film thickness and the stress were measured using a surface profiler (AMBIOS model XP-2, USA). The deposition rate was calculated from the measured film thickness. The deposition rate corresponds to the ratio of the thickness of the thin film to the deposition time with the unit of nm/min. The structural properties of the Ti films were characterized using X-ray diffraction (XRD) employing the PHILIPS model PW 3040 XRD instrument with Cu Kα radiation operated at 30 kV and 30 mA. The scanning was performed in the conventional Bragg diffraction (CBD) mode from 30° to 60°. The surface roughness was determined using atomic force microscopy (AFM; Asylum Research MFP-3D-Bio) in semi-contact (tapping) mode with a scan area of 1 μm × 1 μm. The surface morphology of the Ti films was inspected by scanning electron microscopy (SEM; JEOL, JSM-7800).

Table 1
Electrical parameters (different pulse widths) in the experiment.

Discharge voltage (V)	Frequency (Hz)	Pulse width (μs)	Average power (W)	Peak power (kW)
800	400	40	378	43
		60	739	47
		80	1213	52
		100	1609	51
		120	2079	52
		140	2553	52

Table 2
Electrical parameters (different frequencies) in the experiment.

Discharge voltage (V)	Frequency (Hz)	Pulse Width (μs)	Average power (W)	Peak power (kW)
800	100	100	301	51
	200		701	51
	400		1609	51
	600		2405	51
	800		3138	51

Table 3
Electrical parameters (different trigger pulses) in the experiment.

Discharge voltage (V)	Frequency (Hz)	Pulse width (μs)	Average Power (W)	Peak Power (kW)
600	538	100	1100	28
650	500		1248	33
700	400		1157	42
750	337		1144	45
800	300		1179	51
900	230		1153	64

3. Results

In HPPMS discharges, the target voltage (V) and discharge current (I) are closely related to the plasma characteristics. Fig. 2a shows the voltage and the discharge current characteristics of the Ti target at various average powers. The average power was adjusted by changing the pulse width from 40 μs to 140 μs at a constant discharge of 800 V and frequency of 400 Hz. The V and I oscillogram shown in Fig. 2a indicates that the discharge voltage is 800 V at the beginning of the pulse, and it abruptly decreases to a steady state of ~400 V at the latter part of the pulse. The corresponding discharge current shows a rapid increase to a maximum value of ~160 A at ~60 μs after starting the pulse, and then tends to be stable for most part of the pulse duration. Fig. 2b shows the V and I oscillogram of the Ti target at different average power obtained by adjusting the frequency of the pulses at a constant discharge voltage of 800 V and pulse width of 100 μs. The corresponding discharge current waveform indicates that the plasma ignition time decreases with an increase in frequency. Because at high frequencies, the plasma filling the gap between both electrodes has lesser time to relax [27]. The stray electron from a cycle can help with the ignition of the plasma in the next cycle. Thus, the delay time is shorter at higher frequency. Fig. 2c shows the V and I characteristics of the Ti target at different peak power. In order to maintain the average power constant, frequency was varied from 230 Hz to 538 Hz while the pulse width was maintained at 100 μs during the experiment as shown in Fig. 2c. It was found that the discharge voltage greatly influences the peak current. Therefore, the peak power increases with an increase in the discharge voltage, as shown in Table 3. Meanwhile, ion current can be used as a proxy for the incoming fluxes of species to the substrate, which in turn has a significant effect on the properties of the films. It is worth noting that there is a delay time (about 10 μs) at the beginning of pulse in the ion current curve. This can be ascribed to the time−of−flight for the ions flying from target to substrate. From the curve of ion current, the ion saturation current ion was also recorded to calculate the plasma density, which is described in detailed later.

Fig. 3 a1, b1, and c1 show the OES results of the HPPMS discharge in front of the substrate at different deposition conditions. The OES results indicate that the plasma mainly consists of Ti^+, Ti^0, and Ar^+ emission lines according to the National Institute of Standards and Technology (NIST) Database [28].

Fig. 3 a2 and b2 show the plot of emission intensity ratio versus the average power for different pulsing conditions, and Fig. 3 c2 shows the plot of emission intensity ratio versus the peak discharge power. The emission intensity ratio is defined by the following equation

$$\kappa = \frac{I(Ti^+)}{I(Ti)}, \quad (3)$$

$I(Ti^+)$ is the sum of emission intensities of the spectral lines at 368.5, 375.9, and 376.1 nm, whereas I(Ti) is the sum of emission intensities of the spectral lines observed at 498.1, 499.1, and 499.9 nm. The emission lines of Ti^0 and Ti^+ exhibit similar excitation energies (E_k). Therefore, they were not considered for this analysis in order to avoid the influence of excitation energy on the excitation probability [21] (Table 4). Hence, κ represents a rough estimate of the degree of target material ionization [29] in our analysis, and it is a qualitative indication.

As shown in Fig. 3 a and b, the intensities of four main species, Ti^+, Ti, Ar, and Ar^+ increase with an increase in the pulse width and frequency. Thus, the intensity of every species increases with an increase in the average power. On increasing the discharge voltage (peak power) at a constant average power (shown in Fig. 3 c), the

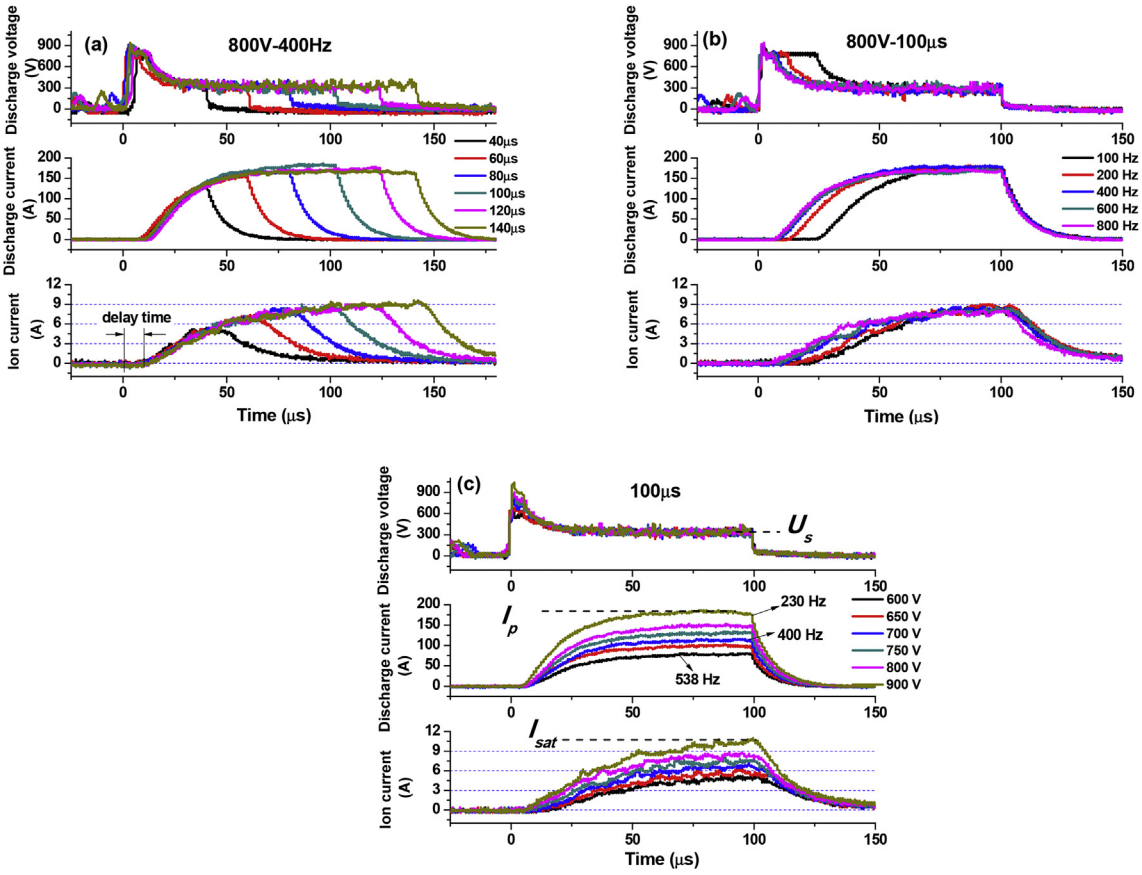

Fig. 2. Target discharge voltage (top panel), the discharge current (middle panel) and the ion current at the substrate (bottom panel) at (a) different pulse widths while keeping the trigger voltage at 800 V and pulse frequency at 400 Hz, (b) different frequencies while keeping the trigger voltage at 800 V and pulse width at 100 μs and (c) different trigger voltages while keeping the pulse width at 100 μs and frequency, and the frequency was varied from 230 Hz to 538 Hz to maintain the average power constant. (Pulsed power supply from Chengdu Pulsetech Electrical).

intensities of ion emission peaks (Ti^+ and Ar^+) show a remarkable increase. The intensities of the emission lines corresponding to Ti atoms decrease faintly, but the intensities of the emission lines corresponding to Ar atoms decrease considerably. As it can be seen in Fig. 3 a2, b2, and c2, no significant change in the emission intensity ratio, κ, of Ti ions is observed by varying pulse width and frequency, although the average power does increase. In addition, it was noted that the plasma sustains for a longer period of time as the pulse width increases. This occurs as atoms would have more chance to collide with the electrons, increasing the ion-to-atom ratio [27]. Therefore, the emission intensity ratio, κ of Ti ions slightly increases from 0.33 to 0.43, as shown in Fig. 3a. By regulating the frequency to control the average power, the discharge current changes a little show little change if any (Fig. 2b), indicating no significant difference in the plasma composition between each pulse. As shown in Fig. 3. b2, the emission intensity ratio of Ti ions is stable at 0.45 without any change. However, κ strongly depends on the discharge voltage (peak power). The emission ratio, κ is significantly high for high peak powers (κ = 0.55), as compared to the discharge achieved with low peak powers (κ = 0.25). Thus, on increasing the discharge voltage (peak power) at a constant average power, the ion-to-atom ratio increases, causing more metal ions to reach the substrate and contribute to the film growth.

Fig. 4 shows the plasma density and gas temperature at different average power and peak power. Using the ion saturation current in Fig. 2, the plasma density can be derived from the calculation formula of the ion saturation current [30] as follows,

$$I_{sat} = 0.61 Sen_0 \left(\frac{kT_e}{m_i}\right)^{1/2}, \quad (4)$$

where I_{sat} is the ion saturation current (A), n_0 is the plasma density (m^{-3}), e is the electron charge (c), S is the effective area of the sheath to collect ions (0.1 * 0.135 m^2), k is Boltzmann's constant, T_e is the electron temperature, and m_i is the ion mass (kg). T_e was assumed to be about 1.5 eV according to literature [21,31]. It is noted that the plasma density increase slightly with an increase in the average power at a constant peak power. However, for cases with constant average power and increasing peak powers, the plasma density has a significant increase, varying from 1.38×10^{18} to 3.06×10^{18} m^{-3}. A higher density downstream leads to a higher ionization fraction of the sputtered material [32].

The gas temperature at the end of deposition was also recorded, which is also shown in Fig. 4 (b). It is interesting to see that the average power has a profound influence on the gas temperature. The temperature around the substrate goes up from 117 °C to 253 °C. However, the gas temperature has decrease slightly as the peak power increases. This difference can be explained by the lower deposition rate at higher peak power resulting in fewer bombarding particles per time unit [33].

The deposition rate of the Ti films deposited at various average power and peak power is shown in Fig. 5. The deposition rate linearly increases with an increase in the average power. Increase in the average power results in substantial ion bombardment to the

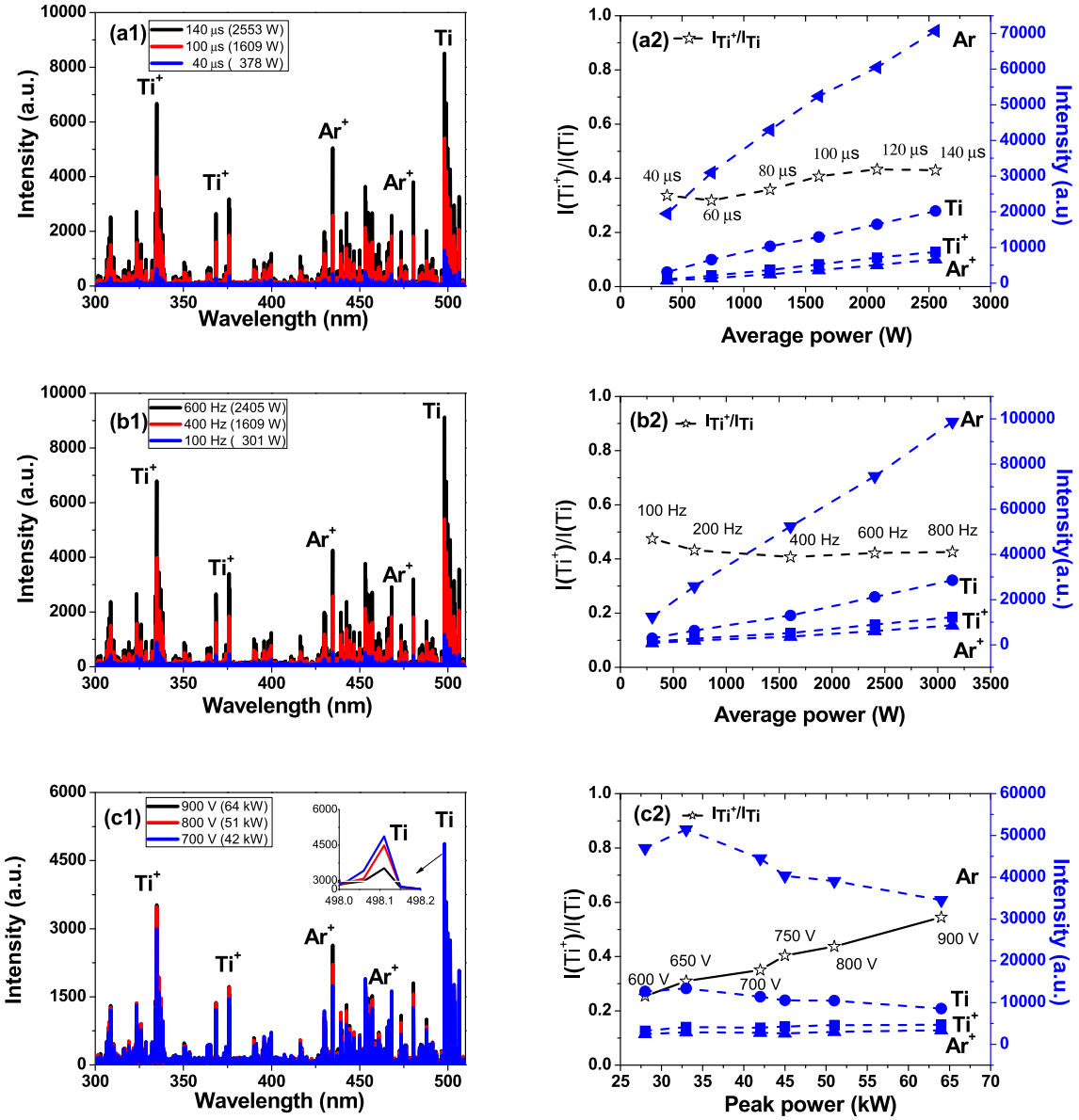

Fig. 3. The OES data of the HPPMS discharge, emission intensity ratio, and the emission spectra intensity of different species at (a) different pulse widths, (b) different frequencies, and (c) different trigger voltages; (I(Ti^+) is the sum of the emission intensities at 368.5, 375.9, and 376.1 nm, I(Ti) is the sum of the emission intensities at 498.1, 499.1, and 499.9 nm, I(Ar^+) is the sum of emission intensities at 434.8 and 466.8 nm, and I(Ar) is the sum of the three emission intensities at 750.4 and 881.5 nm.

Table 4
Selected OES lines for Ti, Ti^+, Ar, and Ar^+.

Ti^+		Ti		Ar^+		Ar	
Wavelength/nm	E_k/eV	Wavelength/nm	E_k/eV	Wavelength/nm	E_k/eV	Wavelength/nm	E_k/eV
368.5	3.96	498.1	3.33	434.8	19.49	750.4	13.47
375.9	3.91	499.1	3.32	466.8	19.80	811.5	13.07
376.1	3.87	499.9	3.30	–	–	–	–

target surface. Therefore, more target atoms are ejected from the target surface. However, the deposition rate is lower in the case of high peak power discharges achieved at a constant average power. This can be attributed to the back-attraction effect [34,35], and the increased trigger voltage does not lead to linear increase in sputter yield [36], which also contributes to lower deposition rate. Apart from the back-attraction of metal ions, the enhanced peak power increases the degree of ionization in the HPPMS discharge, resulting in an increase of bombardment experienced by the growing film by the energetic ions. This re-sputtering effect leads to further reduction in the deposition rates [37]. Meanwhile, the magnetic field topology [38,39] and strength [40–42] on the target surface affect the electric potential distribution in the plasma, leading to low deposition rates.

Fig. 6 shows the surface profilometry measurements (Fig. 6 a1, b1) and the residual stress values (Fig. 6 a2, b2) at various average

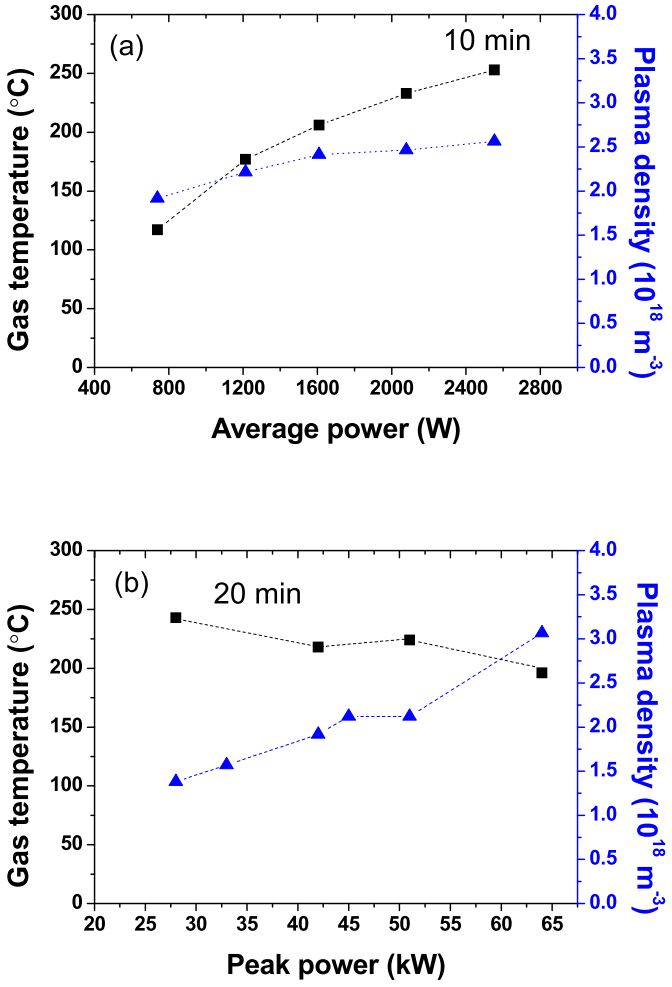

Fig. 4. Plasma density and gas temperature around the substrate at (a) different average powers (pulse widths) at constant peak power and (b) different peak powers (trigger voltages) at a constant average power; (The recording time of gas temperature depends on the deposition time, 10 min is Fig. a and 20 min in Fig. b).

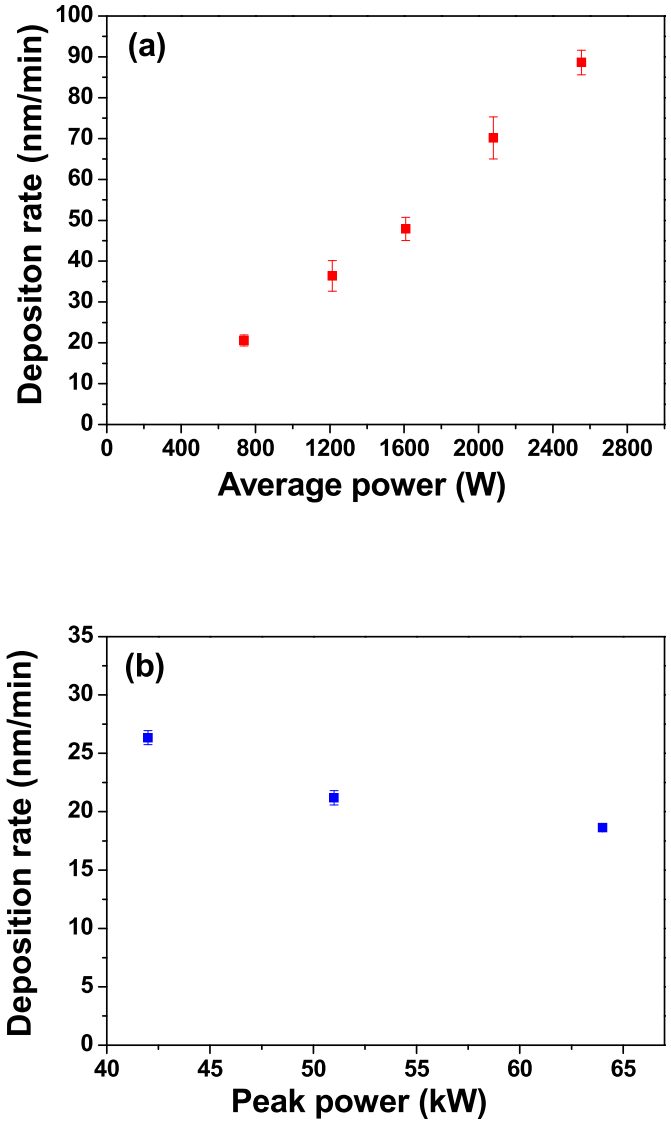

Fig. 5. Deposition rate at (a) different average powers with constant peak power and (b) different peak powers with constant average power.

and peak powers. The residual stress values were calculated using the Stoney's equation [43] based on wafer curvature [44] measurements, and the thermal stress has been subtracted based on the method in Ref. [45]. For a fixed peak power of ~50 kW, the Ti films exhibit tensile stress with changes in the average power. The magnitude of the tensile stress increases as the average power increases from 1213 W to 2553 W. However, on regulating the peak power at a constant average power, the Ti films exhibit compressive stress at higher peak powers. The residual stress of the film is changed from tensile to compressive when the peak power is increased from 42 kW to 64 kW.

XRD θ/2θ patterns of the Ti films obtained at different average and peak powers are shown in Fig. 7. XRD spectra reveal that the Ti films are polycrystalline and exhibit a hexagonal structure. All spectra obtained from our experiments are in good agreement with the standard data for Ti (JCPDS No. 03-065-6231). Typically, Ti films exhibit a close-packed hexagonal structure and (002) is the most stable configuration in our films as it has the lowest surface energy [46]. The Ti films deposited at different conditions contain mixed crystalline orientations of (100), (002), and (101) with (002) as the preferred orientation. With an increase in the average power, the Ti films exhibit a highly preferred (002) direction and sharper peak intensity, this can be ascribed to the higher deposition rate in the case of higher average power. The higher deposition rate leads to a smaller nucleation distance, resulting in the sputtered adatoms that can easily move and reach energetically favorable adsorption site on the lowest surface free energy plane (002) [47]. However, for high peak power discharges at a constant average power, the peak corresponding to (002) exhibits low diffraction intensity. This is because the grain growth toward the close-packed direction can be suppressed by the energetic ion bombardment during deposition. The close-packed plane incurs more collision damage than the less densely packed plane, resulting in the preferential development of the unusual crystalline orientation [48]. In addition, the full width at half maximum (FWHM) increases with an increase in the peak power. This is caused by both the microstress and the decrease of grain size. The exact peak positions of (002) of Ti films are shown in Table 5. It is noted that the (002) peak of films has a shift to lower Bragg's diffraction angle with the peak power increasing, indicating the Ti films tends to be in subject to compressive stress. When the average power increases from 1609 W to 2553 W, the (002) peak in the films has a shift to higher diffraction angle, this suggests the Ti films show a higher tensile stress. As the tensile stress of film

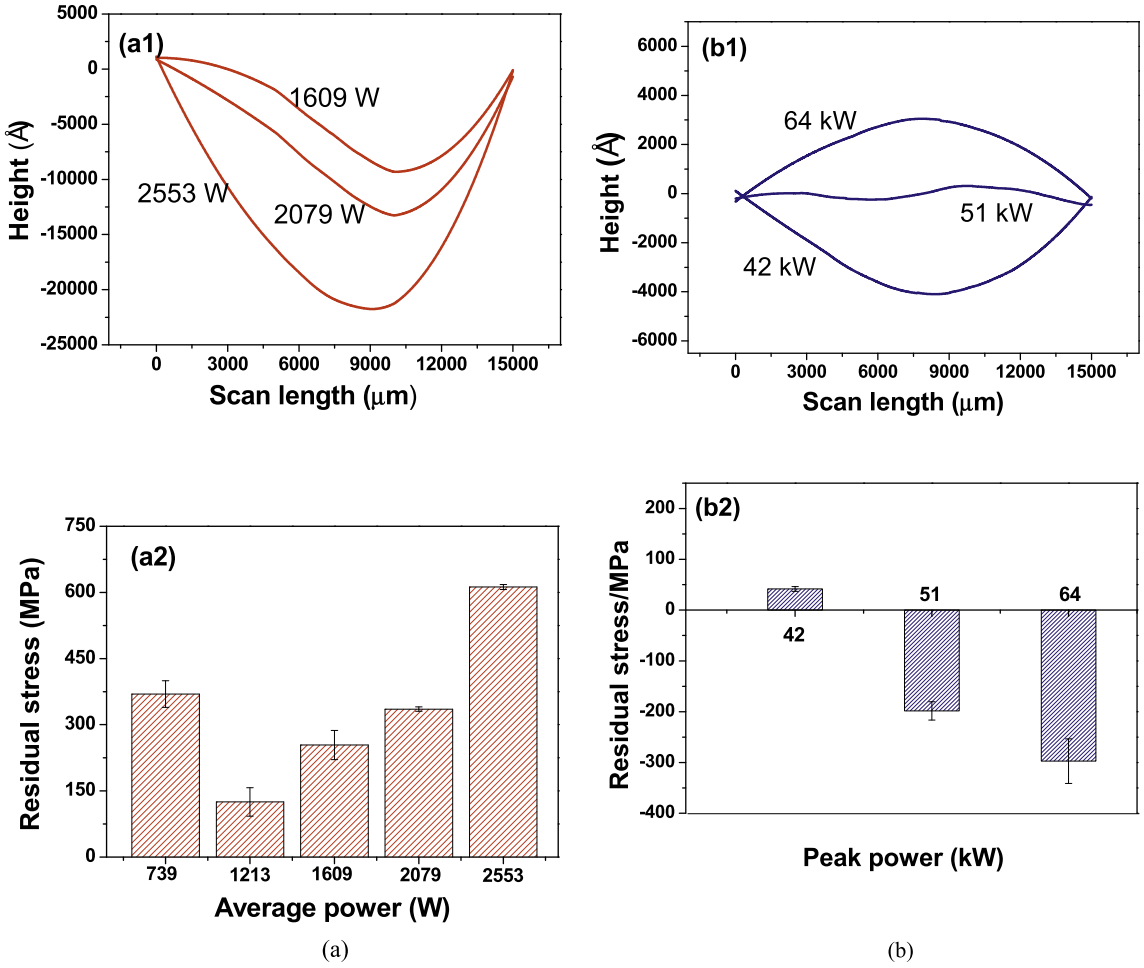

Fig. 6. (a1), (b1) Deformation profiles of Si substrates and (a2), (b2) residual stress calculated with the Stoney's equation at different average power and peak power (The thermal stress was subtracted based on the method in the reference [45]).

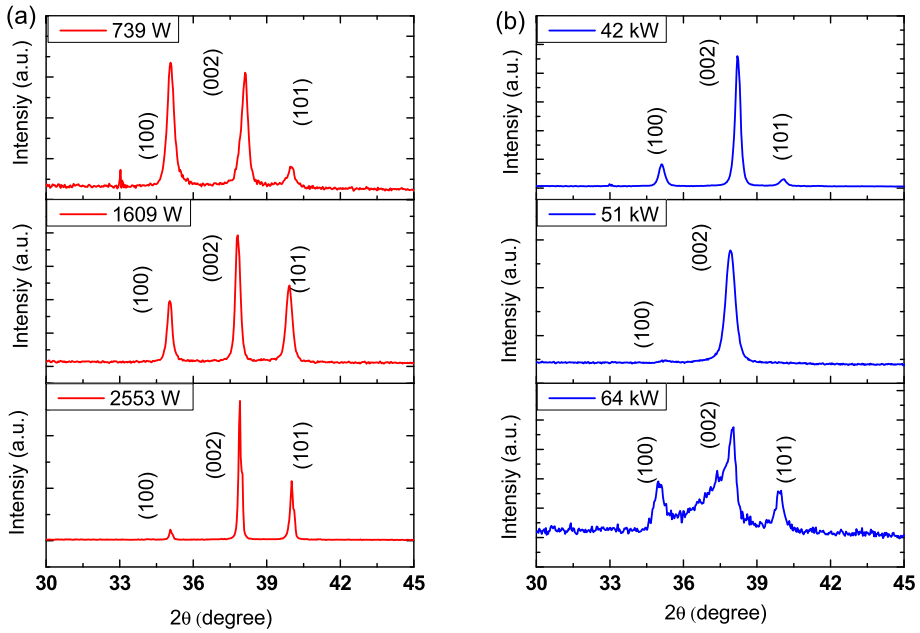

Fig. 7. XRD pattern of the samples obtained at different (a) different average power with constant peak power and (b) different peak power with constant average power.

Table 5
The exact peak position of (002) of Ti films.

Peak power (kW)	(002)-2θ (degree)	Average power (W)	(002)-2θ (degree)
42	38.19	739	38.14
51	37.97	1609	37.82
64	37.95	2553	37.90

prepared at 739 W is larger than that prepared at 1609 W, shown in Fig. 6 (a2). So the diffraction angle of (002) peak of the films prepared at 739 W is larger than that of the one obtained at 1609 W.

Furthermore, the surface morphology of the Ti films was investigated using AFM and SEM. Fig. 8 shows the three-dimensional AFM images of the Ti films deposited on Si wafers at different average and peak powers, separately. The surface roughness increases with an increase in the average power. For a high average power of 2553 W, the film is characterized by large granular structures and a surface roughness of 1.77 nm. On the contrary, for higher peak powers of 64 kW (at a constant average power), the film surface is characterized by smaller grains, and the sample exhibit a relatively smooth surface with a surface roughness of 0.56 nm. The surface topography of Ti films obtained at different average power and peak power is shown in Fig. 9. It is noted that the granular structure becomes larger as the average power increases (shown in Fig. 9 a). For a higher average power of 2553 W, the film is characterized by higher roughness. On the contrary, for higher peak powers of 64 kW (at a constant average power), the films tend to be smooth and dense, and the granular structure is smaller than the one prepared by lower peak power 42 kW (shown in Fig. 9 b). These results are consistent with the results of AFM.

4. Discussion

In this study, the deposition rate, surface roughness, grain size, and residual stress of Ti films were successfully tailored by changing the peak and average powers employed in the HPPMS discharge. An illustration (Fig. 10) of the change of film properties with an increase in the average power or peak power is used to summarize the results obtained from this study. The changes in the film properties are closely related to the plasma characteristics, especially to the plasma composition around the substrate achieved during the HPPMS discharge. The increase in the average power of the discharge has a negligible effect on the emission intensity ratio, κ of Ti ions. However, the overall intensities of Ar^+, Ar, Ti, and Ti^+ increase with an increase in the average power. With an increase in the average power, more Ti species are sputtered and deposited on the substrate, and hence, the deposition rate increases as shown in Fig. 5a. The peak power, however, greatly influences the ion-to-atom ratio to the substrate when the average power is kept constant. The emission intensity ratio, κ of Ti ions increases from ~0.25 to ~0.55 with an increase in the peak power. The increase in the peak power results in an increase in the plasma density (shown in Fig. 4 b). A large amount of electrons with a high energy collides with neutral atoms (Ti and Ar) [49], causing a significant fraction of the sputtered target material (Ti) to be ionized as reported previously [22,50,51].

Higher ion flux at higher energies to the substrate would result in a more efficient momentum transfer to the adatoms, which results in increased adatom mobility and smoothening effect [52]. Additionally, the higher ion flux causes repeated nucleation at the substrate, leading to the formation of smaller grains with a smoother surface. Therefore, the surface roughness and grain size of the Ti films exhibit a remarkable drop with an increase in the ion-to-atom ratio of the flux incident on substrate. According to the XRD results (Fig. 7 b), the Ti films deposited at higher peak power values exhibit a lower diffraction intensity and higher FWHM of the (002) peak, as compared with the samples obtained with lower peak power. So the average grain size decreases at high peak powers according to the Scherrer Equation, which is consistent with the results of AFM.

The residual stress in the Ti films becomes compressive as the peak power increases. The intrinsic stress of the film can be tensile or compressive depending on the energetics of the deposition process [53,54]. The low peak power discharge leads to the formation of films with rough microstructures, as energetic particle bombardment is not involved in the fabrication. This results in the development of tensile stress [55] in the growing film. As the peak power increases, the relative ionization rate in the plasma increases, resulting in the occurrence of energetic particle bombardment during the film growth. Increase in the amount of ion flux at higher energies results in the formation of finer grains and denser films. Therefore, the films tend to exhibit compressive stress. However, the Ti films exhibit tensile stress with changes in the average power of the HPPMS discharge. The Ti films exhibit bigger granular structures with rougher surfaces at higher average powers. This could be attributed to the fact that the gas

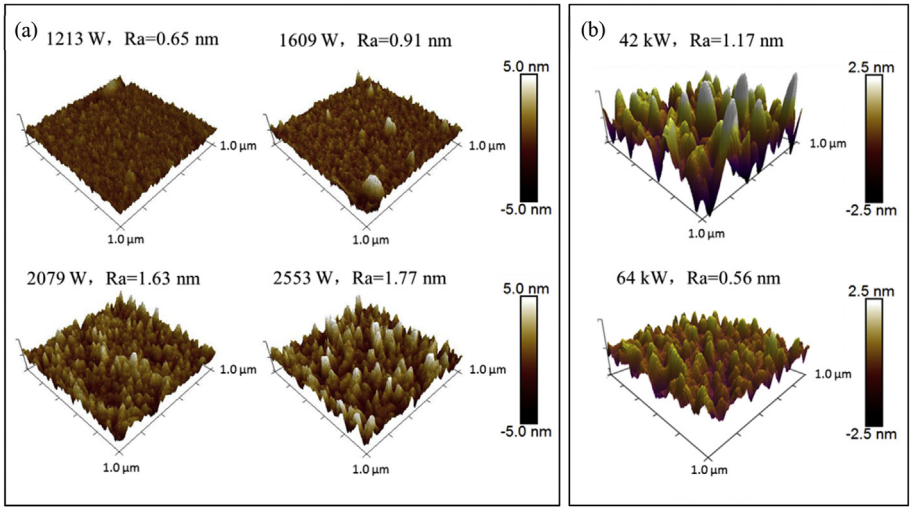

Fig. 8. AFM images of the samples obtained at different (a) different average power with constant peak power and (b) different peak power with constant average power.

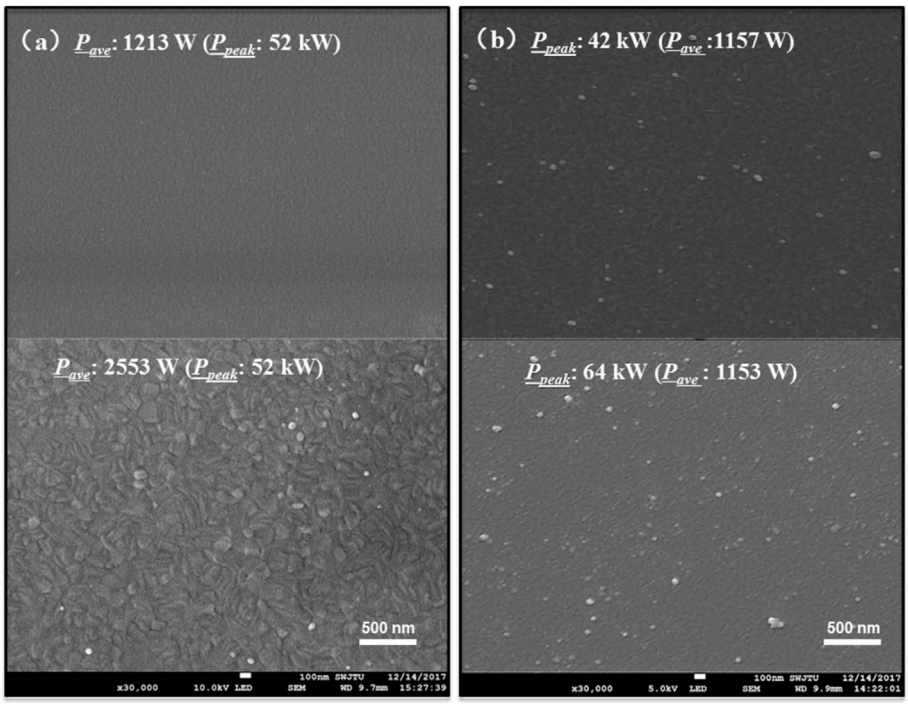

Fig. 9. The surface topography of Ti films obtained at (a) different average power with constant peak power and (b) different peak power with constant average power.

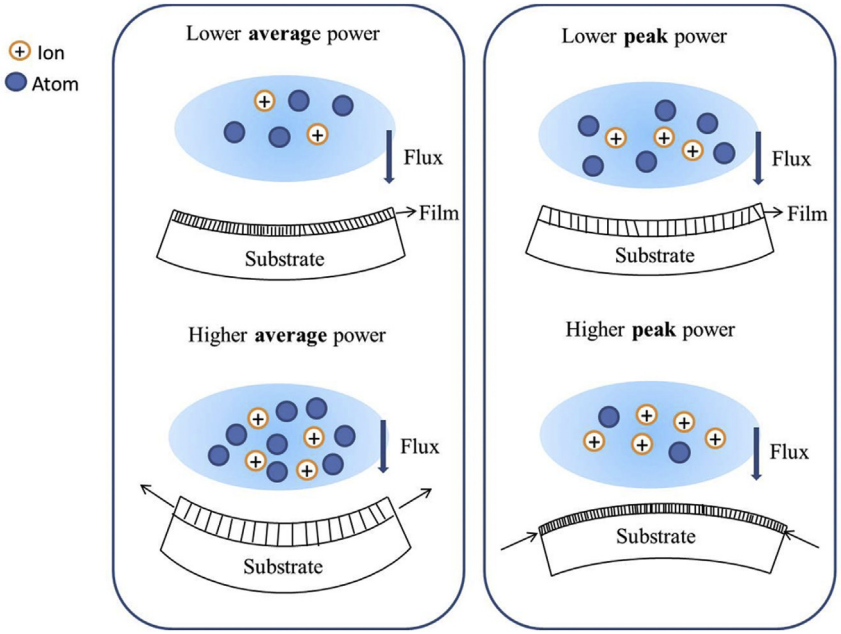

Fig. 10. Illustration of the change of film properties with an increase in the average power or peak power.

temperature around the substrate is higher at higher average power (shown in Fig. 4 a), resulted in the grain growth [5]. The coalescing of the boundaries enhances the volume subtraction, making the film more tensile [56–58]. Besides grain coalescence, the elimination of voids and annihilation of other defects caused by high power might also be an important reason for tensile stress [59]. The flux of Ti species arriving at the surface of the substrate is higher owing to the higher deposition rates. Consequently, surface roughness increases due to the atomic shadowing [60], and more number of nuclei are formed on the surface, leading to the formation of bigger grains [61]. This is in accord with our results shown in Fig. 7a. XRD patterns of the samples obtained with higher average power reveal narrower peak width at the half height, which is indicative of larger crystal sizes.

In summary, the films properties are closely related to the ion-to-atom ratio in the material flux incident at the substrate. The increase in the peak power results in an increase in the ion-to-atom ratio, thereby resulting in increased ion bombardment to the growing film. Target (Ti) ions arrive at the substrate at higher energy owing to the acceleration occurring at the plasma sheath.

Therefore, the films deposited at higher peak powers tend to exhibit compressive stress, smaller grain size, and smoother surface at lower deposition rates. The ion-to-atom ratio remains almost constant with an increase in the average power, but the magnitude of the number of ions and atoms and gas temperature around the substrate increases. This results in higher deposition rates and higher substrate temperatures, which in turn results in rougher films exhibiting tensile stress and large grain size. Our results clearly emphasize the importance of choosing proper HPPMS process parameters to achieve desirable film properties.

5. Conclusion

In this study, Ti films were deposited using an HPPMS technique at different average and peak target powers. The deposition rate, roughness, grain size, residual stress, and microstructure of the deposited were successfully tailored. Target current-voltage characteristics and plasma composition were monitored during the deposition. The increase in the discharge voltage causes a significant increase in the peak power, thereby resulting in a high plasmas density and ion-to-atom ratio. The films deposited at higher peak powers tend to exhibit compressive stress and denser and smoother microstructure at lower deposition rates. Increasing the pulse width and frequency is beneficial for increasing the average power, thereby effectively increasing the gas temperature around the substrate and deposition rates. The films deposited at higher average powers exhibit tensile stress and large grain size with a rougher surface. Hence, the plasma density, temperature around the substrate and ion-to-atom ratio and are controlled by controlling various average or peak power, which is beneficial for achieving thin films with desirable properties. Therefore, a careful selection of HPPMS power parameters leads to the efficient tailoring of thin film properties.

Acknowledgments

This work was supported by NSAF (Grant No. U1330113), NSFC (31300787), and Doctoral Innovation Fund Program of Southwest Jiaotong University. The authors gratefully acknowledge the financial support from the China Scholarship Council. Many thanks for the kind suggestions from Dr. Yuhua Sun, Dr. Priya Raman and Dhruval Patel.

References

[1] S. Venkatesan, M. Ramu, Influence of controlled deposition rate on mechanical properties of sputtered Ti thin films for MEMS application, Mater. Sci.-Poland (2016) 34.
[2] Y.H. Joo, N.-H. Kim, Characteristics of Ti thin films and application as a working electrode in TCO-less dye-sensitized solar cells, Trans. Electr. Electron. Mater. 18 (2017) 93–96.
[3] M. Einollahzadeh-Samadi, R.S. Dariani, Growth mechanism and optical properties of Ti thin films deposited onto fluorine-doped tin oxide glass substrate, J. Vac. Sci. Technol.: Vac. Surf. Films 33 (2015), 021403.
[4] J. Jaiswal, A. Sanger, A. Kumar, S. Mourya, S. Chauhan, R. Daipuriya, et al., Enhanced optical absorbance of hydrophobic Ti thin film: role of surface roughness, Adv. Mater. Lett. 7 (2016) 485–490.
[5] M. Einollahzadeh-Samadi, R.S. Dariani, Effect of substrate temperature and deposition rate on the morphology and optical properties of Ti films, Appl. Surf. Sci. 280 (2013) 263–267.
[6] N. Muslim, Y.W. Soon, C.M. Lim, N.Y. Voo, Influence of sputtering power on properties of titanium thin films deposited by RF magnetron sputtering, J. Eng. Appl. Sci. 10 (2015) 7184–7189.
[7] K.N. Chappanda, Y.R. Smith, L.W. Rieth, P. Tathireddy, M. Misra, S.K. Mohanty, Effect of sputtering parameters on the morphology of TiO_2 nanotubes synthesized from thin Ti film on Si substrate, IEEE Trans. Nanotechnol. 14 (2015) 18–25.
[8] S. Chen, B.H. Wu, D. Xie, F. Jiang, J. Liu, H.L. Sun, et al., The adhesion and corrosion resistance of Ti–O films on CoCrMo alloy fabricated by high power pulsed magnetron sputtering (HPPMS), Surf. Coating. Technol. 252 (2014) 8–14.
[9] M. Hu, S. Noda, T. Okubo, Y. Yamaguchi, H. Komiyama, Structural and morphological control of nanosized Cu islands on SiO_2 using a Ti underlayer, J. Appl. Phys. 94 (2003) 3492.
[10] Z. Soukup, J. Lhotka, J. Musil, D. Rafaja, Effect of Ti interlayer and bias on structure and properties of TiN films, Czech. J. Phys. 50 (2000) 655–663.
[11] J.-H. Huang, F.-Y. Ouyang, G.-P. Yu, Effect of film thickness and Ti interlayer on the structure and properties of nanocrystalline TiN thin films on AISI D2 steel, Surf. Coating. Technol. 201 (2007) 7043–7053.
[12] J.-H. Huang, C.-H. Ma, H. Chen, Effect of Ti interlayer on the residual stress and texture development of TiN thin films, Surf. Coating. Technol. 200 (2006) 5937–5945.
[13] D.-S. Park, Y.-H. Kim, Texture enhancement of Al films on Ti underlayers by radio-frequency bias sputtering, J. Electron. Mater. 31 (2002) 1009–1015.
[14] V. Kouznetsov, K. Macák, J.M. Schneider, U. Helmersson, I. Petrov, A novel pulsed magnetron sputter technique utilizing very high target power densities, Surf. Coating. Technol. 122 (1999) 290–293.
[15] G. Greczynski, J. Jensen, J. Böhlmark, L. Hultman, Microstructure control of CrNx films during high power impulse magnetron sputtering, Surf. Coating. Technol. 205 (2010) 118–130.
[16] J. Bohlmark, J. Alami, C. Christou, A.P. Ehiasarian, U. Helmersson, Ionization of sputtered metals in high power pulsed magnetron sputtering, J. Vac. Sci. Technol.: Vac. Surf. Films 23 (2005) 18.
[17] K. Sarakinos, J. Alami, S. Konstantinidis, High power pulsed magnetron sputtering: a review on scientific and engineering state of the art, Surf. Coating. Technol. 204 (2010) 1661–1684.
[18] A. Anders, Discharge physics of high power impulse magnetron sputtering, Surf. Coating. Technol. 205 (2011) S1–S9.
[19] N. Bagcivan, K. Bobzin, G. Grundmeier, M. Wiesing, O. Ozcan, C. Kunze, et al., Influence of HPPMS pulse length and inert gas mixture on the properties of (Cr,Al)N coatings, Thin Solid Films 549 (2013) 192–198.
[20] K. Bobzin, T. Brögelmann, R.H. Brugnara, Aluminum-rich HPPMS (Cr1−xAlx)N coatings deposited with different target compositions and at various pulse lengths, Vacuum 122 (2015) 201–207.
[21] A.P. Ehiasarian, A. Vetushka, Y.A. Gonzalvo, G. SÁfrán, L. Székely, P.B. Barna, Influence of high power impulse magnetron sputtering plasma ionization on the microstructure of TiN thin films, J. Appl. Phys. 109 (2011) 104314.
[22] J. Alami, K. Sarakinos, F. Uslu, M. Wuttig, On the relationship between the peak target current and the morphology of chromium nitride thin films deposited by reactive high power pulsed magnetron sputtering, J. Phys. Appl. Phys. 42 (2009), 015304.
[23] G. Greczynski, L. Hultman, Peak amplitude of target current determines deposition rate loss during high power pulsed magnetron sputtering, Vacuum 124 (2016) 1–4.
[24] G. Greczynski, J. Jensen, L. Hultman, Mitigating the geometrical limitations of conventional sputtering by controlling the ion-to-neutral ratio during high power pulsed magnetron sputtering, Thin Solid Films 519 (2011) 6354–6361.
[25] B.H. Wu, Y. Wang, Y. Yu, F. Jiang, H. Sun, F.J. Jing, et al., Modulate the deposition rate through changing the combination of frequency and pulse width at constant duty cycle, Surf. Coating. Technol. 281 (2015) 27–34.
[26] B.H. Wu, J. Wu, F. Jiang, D.L. Ma, C.Z. Chen, H. Sun, et al., Plasma characteristics and properties of Cu films prepared by high power pulsed magnetron sputtering, Vacuum 135 (2017) 93–100.
[27] S. Konstantinidis, J.P. Dauchot, M. Ganciu, A. Ricard, M. Hecq, Influence of pulse duration on the plasma characteristics in high-power pulsed magnetron discharges, J. Appl. Phys. 99 (2006), 013307.
[28] Kramida A, Ralchenko Y, Reader J, Team NA. NIST Atomic Spectra Database. Gaithersburg: National Institute of Standards and Technology.
[29] J. Čapek, M. Hála, O. Zabeida, J.E. Klemberg-Sapieha, L. Martinu, Deposition rate enhancement in HiPIMS without compromising the ionized fraction of the deposition flux, J. Phys. Appl. Phys. 46 (2013) 205205.
[30] T.M. Minea, C. Costin, A. Revel, D. Lundin, L. Caillault, Kinetics of plasma species and their ionization in short-HiPIMS by particle modeling, Surf. Coating. Technol. 255 (2014) 52–61.
[31] A. Vetushka, A.P. Ehiasarian, Plasma dynamic in chromium and titanium HIPIMS, J. Phys. D Appl. Phys.: Appl. Phys. 41 (2008), 015204.
[32] L. Meng, H. Yu, M.M. Szott, J.T. McLain, D.N. Ruzic, Downstream plasma transport and metal ionization in a high-powered pulsed-plasma magnetron, J. Appl. Phys. 115 (2014) 223301.
[33] G. West, P. Kelly, P. Barker, A. Mishra, J. Bradley, Measurements of deposition rate and substrate heating in a HiPIMS discharge, Plasma Process. Polym. 6 (2009) S543–S547.
[34] D.J. Christie, Target material pathways model for high power pulsed magnetron sputtering, J. Vac. Sci. Technol.: Vac. Surf. Films 23 (2005) 330.
[35] D.J. Christie, Fundamentals of high power pulsed magnetron sputtering: visualization of mechanisms for rate reduction and increased ion fraction, Czech. J. Phys. 56 (2006) B93–B97.
[36] J. Emmerlich, S. Mráz, R. Snyders, K. Jiang, J.M. Schneider, The physical reason for the apparently low deposition rate during high-power pulsed magnetron sputtering, Vacuum 82 (2008) 867–870.
[37] F.J. Jing, T.L. Yin, K. Yukimura, H. Sun, Y.X. Leng, N. Huang, Titanium film deposition by high-power impulse magnetron sputtering: influence of pulse duration, Vacuum 86 (2012) 2114–2119.
[38] P. Raman, I.A. Shchelkanov, J. McLain, D.N. Ruzic, High power pulsed magnetron sputtering: a method to increase deposition rate, J. Vac. Sci. Technol.: Vac. Surf. Films 33 (2015), 031304.

[39] P. Raman, I. Shchelkanov, J. McLain, M. Cheng, D. Ruzic, I. Haehnlein, et al., High deposition rate symmetric magnet pack for high power pulsed magnetron sputtering, Surf. Coating. Technol. 293 (2016) 10–15.
[40] J. Wu, B.H. Wu, D.L. Ma, D. Xie, Y.P. Wu, C.Z. Chen, et al., Effects of magnetic field strength and deposition pressure on the properties of TiN films produced by high power pulsed magnetron sputtering (HPPMS), Surf. Coating. Technol. 315 (2017) 258–267.
[41] A. Mishra, P.J. Kelly, J.W. Bradley, The evolution of the plasma potential in a HiPIMS discharge and its relationship to deposition rate, Plasma Sources Sci. Technol. 19 (2010), 045014.
[42] J.W. Bradley, A. Mishra, P.J. Kelly, The effect of changing the magnetic field strength on HiPIMS deposition rates, J. Phys. Appl. Phys. 48 (2015) 215202.
[43] G.G. Stoney, The tension of metallic films deposited by electrolysis, Proc. Roy. Soc. Lond.: Math. Phys. Eng. Sci. 82 (1909) 172–175.
[44] F. Jiang, S. Chen, Y. Leng, N. Huang, Effect of wafer size on the film internal stress measurement by wafer curvature method, J. Wuhan Univ. Technol.-Materials Sci. 31 (2016) 93–99.
[45] G. Greczynski, J. Lu, S. Bolz, W. Kölker, C. Schiffers, O. Lemmer, et al., Novel strategy for low-temperature, high-rate growth of dense, hard, and stress-free refractory ceramic thin films, J. Vac. Sci. Technol.: Vac. Surf. Films 32 (2014), 041515.
[46] R. Checchetto, Titanium thin film deposition in a deuterium atmosphere, Thin Solid Films 302 (1997) 77–83.
[47] A.Y. Chen, Y. Bu, Y.T. Tang, Y. Wang, F. Liu, X.F. Xie, et al., Deposition-rate dependence of orientation growth and crystallization of Ti thin films prepared by magnetron sputtering, Thin Solid Films 574 (2015) 71–77.
[48] W. Ensinger, On the mechanism of crystal growth orientation of ion beam assisted deposited thin films, Nucl. Instrum. Methods Phys. Res. Sect. B Beam Interact. Mater. Atoms 106 (1995) 142–146.
[49] J.T. Gudmundsson, Ionization mechanism in the high power impulse magnetron sputtering (HiPIMS) discharge, J. Phys. Conf. 100 (2008), 082013.
[50] C. Nouvellon, M. Michiels, J.P. Dauchot, C. Archambeau, F. Laffineur, E. Silberberg, et al., Deposition of titanium oxide films by reactive High Power Impulse Magnetron Sputtering (HiPIMS): influence of the peak current value on the transition from metallic to poisoned regimes, Surf. Coating. Technol. 206 (2012) 3542–3549.
[51] D. Lundin, M. Čada, Z. Hubička, Ionization of sputtered Ti, Al, and C coupled with plasma characterization in HiPIMS, Plasma Sources Sci. Technol. 24 (2015), 035018.
[52] S. Mahieu, P. Ghekiere, G. De Winter, R. De Gryse, D. Depla, G. Van Tendeloo, et al., Biaxially aligned titanium nitride thin films deposited by reactive unbalanced magnetron sputtering, Surf. Coating. Technol. 200 (2006) 2764–2768.
[53] H. Windischmann, Intrinsic stress in sputter-deposited thin films, Crit. Rev. Solid State Mater. Sci. 17 (1992) 547–596.
[54] I.-L. Velicu, V. Tiron, C. Porosnicu, I. Burducea, N. Lupu, G. Stoian, et al., Enhanced properties of tungsten thin films deposited with a novel HiPIMS approach, Appl. Surf. Sci. 424 (2017) 397–406.
[55] Y. Pauleau, Generation and evolution of residual stresses in physical vapour-deposited thin films, Vacuum 61 (2001) 175–181.
[56] D. Magnfält, Nucleation and Stress Generation in Thin Films Deposited with a Pulsed Energetic Deposition Flux, Linköping University, Sweden, 2013.
[57] P. Chaudhari, Grain growth and stress relief in thin films, J. Vac. Sci. Technol. 9 (1972) 520.
[58] S.C. Seel, C.V. Thompson, S.J. Hearne, J.A. Floro, Tensile stress evolution during deposition of Volmer–Weber thin films, J. Appl. Phys. 88 (2000) 7079.
[59] S. Zhou, W. Wu, T. Shao, Effect of post deposition annealing on residual stress stability of gold films, Surf. Coating. Technol. 304 (2016) 222–227.
[60] I. Petrov, P.B. Barna, L. Hultman, J.E. Greene, Microstructural evolution during film growth, J. Vac. Sci. Technol.: Vac. Surf. Films 21 (2003), S117.
[61] K. Bordo, H.-G. Rubahn, Effect of deposition rate on structure and surface morphology of thin evaporated Al films on dielectrics and semiconductors, Mater. Sci. 18 (2012) 313–317.